COMMUNICATION

Check for updates

An all-solid-state biocompatible ion-to-electron transducer for bioelectronics†

M. Sheliakina, [iD] [a] A. B. Mostert [iD] [a] and P. Meredith [iD] *[b]

Reported here is an all-solid-state organic electrochemical transistor based on the biopolymer melanin. The underlying mechanism is demonstrated using a unique hydration dependence protocol and explained using an adapted double capacitor model. The demonstration of an all-solid-state bioelectronic prototype is critical for the development of miniaturised bioelectronic logic.

Conceptual insights

Bioelectronics is an emergent field at the intersection of the life and physical sciences which seeks to connect biological entities with conventional electronics, and in so doing create new medical therapies. One of the key, underlying challenges in bioelectronics is to transduce between the predominantly ionic signals of biology and the electronic signals of semiconductor electronics. To this end, we demonstrate a novel all solid-state transducing interface based upon the proton conducting biopolymer melanin, and a p-type organic electrochemical transistor. This device has a channel length of 100 μm, ON/OFF ratios as high as 10^4 and operates at <1 V. As such, it is a significant advance on the pathway to full bioelectronic logic – that is, devices that can compute at the biology–electronic interface. Furthermore, we show unequivocally that our transducer operates *via* so-called volumetric gating, a pre-requisite for further miniaturisation, fast response times and lower power operation. Finally, we advance a new double volumetric capacitor model to fully explain the gating and transistor behaviour. We also note this is the first viable, functioning electronic device constructed from the important biopolymer melanin after decades of attempts.

Introduction

Bioelectronics

Bioelectronics is a rapidly emerging field at the intersection of the physical, chemical and life sciences which seeks to create new medical interventions, biosensors, monitoring devices *etc.* by directly reading or writing biological signals with conventional semiconductor-based electronics.[1–9] In biology, electrical currents are primarily driven by the flow of ions (the smallest of which is the proton), rather than electrons, which are the charge carriers in semiconductors and metals. The physics of both ion currents and electron currents are individually very well understood – albeit it from quite different perspectives and by different scientific communities. Ions are large effective mass entities that are usually treated classically: for example utilizing the Stokes–Einstein Relation, classical thermodynamics, and the interplay of ion motion with large scale material structural perturbations.[10,11] Electrons are quantum mechanical entities whose motions are strongly affected by local structure and disorder as famously articulated by Mott & Davis.[12] There are certain cross-over elements in their physics, for example considerable evidence is emerging that protons can 'tunnel',[13] and electrons when strongly localized can 'hop' almost classically site-to-site.[14] However, in the main, the two charge carriers

remain disconnected and their common behaviour and collective transport largely unexplored especially in the solid-state.[2]

Bioelectronic devices and organic electrochemical transistors

Connecting ion and electron currents or 'transducing' between the signals that they carry is non-trivial because of this disconnect in their basic physics. Materials that support high number density, high mobility ion currents in the solid-state are few and far between – ion transport membranes like Nafion and other polymer electrolytes are limited examples.[11,15–18] Conductors that efficiently carry both ion and electron currents are even rarer. Hence, transduction strategies have mainly focused on devices that couple two media/materials together, each preferentially hosting one carrier type, rather than a single media supporting both as evidenced by reviews on multiple device platforms.[1,3,4] Suitable device architectures for creating this transducing interface between the two materials include bipolar ion junctions,[19] membrane coated nanowires,[20,21] proton field effect transistors,[22] and arguably the most mature and

[a] Centre for Organic Photonics and Electronics, School of Mathematics and Physics, University of Queensland, Brisbane, QLD 4072, Australia

[b] Department of Physics, Swansea University, Singleton Park, Swansea SA28PP, Wales, UK. E-mail: paul.meredith@swansea.ac.uk

† Electronic supplementary information (ESI) available. See DOI: 10.1039/c7mh00831g

studied technology – organic electrochemical transistors (OECT).[8] OECTs were first demonstrated by White *et al.*[23] in a device where the conductivity of a film of the semiconducting polymer poly-pyrrole was modulated by the application of a gate voltage through a liquid electrolyte. This delivered 'field effect transistor-like' behaviour. However, state-of-the-art OECTs now utilize the p-type semiconducting polymer poly(3,4-ethylenedioxythiophene) doped with poly(styrenesulfonate) (PEDOT:PSS). The transistor channel conductance in such devices can be modulated by the injection of ions from a liquid electrolyte gate. These ions dope/de-dope the PEDOT backbone and this provides the transducing mechanism. Such OECTs have been used in the detection of ion channels in a bilayer lipid membrane,[24] ions,[25] enzymes,[26] antibodies,[27] DNA,[28] and have also been recently tested in biomedical settings such as electroencephalography, electrooculography and electrocardiography.[29] Another key advantage of the OECT architecture lies in the basic operating mechanism – OECTs gate *via* volumetric capacitance whereby the gating ions interact with electrons in the volume of the channel. This overcomes the limits of surface or inductive gating inherent in field effect transistors, where a maximum capacitance of ≈ 5 F cm^{-3} has a serious impact on responsivity as the channel dimensions are reduced to sizes necessary for large scale integration.

An important recent example of a device operating in volumetric capacitance mode is the so called electrochemical neuromorphic organic device (ENODe), an organic electrochemical artificial synapse of van der Burgt *et al.*[30] The ENODe consists of a PEDOT:PSS (presynaptic electrode)-electrolyte-PEDOT:PSS/polyethylenimine [PEI] (postsynaptic electrode) sandwich which functions as a non-volatile redox cell. The device works by modulation of the postsynaptic electrode conductance due to injection of cations from the electrolyte under application of a positive bias to the presynaptic electrode. Whilst not strictly an OECT, this ENODe demonstrates many non-volatile and stable states at low voltage. Its function appears critically reliant upon direct injection of cations into the PEDOT:PSS/PEI electrode and de-doping of the PEDOT back bone to reduce the conductivity.

Returning to transistor architectures, state-of-the-art OECTs are intrinsically limited by the liquid electrolytic gate. Although the biological environment is 'wet and warm', any read–write–sense device should ideally be all solid-state from the perspectives of stability, long term operation, reproducibility and very importantly, miniaturization and integration. The ultimate goal is to create bioelectronic interfaces which could not only perform read–write functions but also amplify, signal process or even compute.[31] This requires the combination and large scale integration of literally millions of individual components and the realization of low power consumption bioelectronic logic. The use of electrolytic or ionic gels or liquids as transducing gates is likely not compatible with such a vision, and hence the realization of scalable all-solid-state architectures is now a priority in bioelectronics.

Our work is motivated by this priority. To that end, we demonstrate a functional, all-solid-state organic electrochemical p-type transistor with a proton injecting top gate made from the conducting bio-macromolecule eumelanin (simply 'melanin' hereafter).
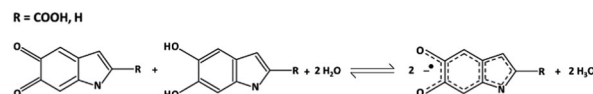

R = COOH, H

Fig. 1 The comproportionation reaction, which dominates melanin electrochemistry. Quinone and hydroquinone moieties react with water to form semiquinones and hydronium.

Melanin as bioelectronic material

Melanin is a ubiquitous functional material in the biosphere[32] and has been recently shown to support predominantly protonic currents in the solid state including thin films of device quality.[33–35] Melanin is the human pigment providing photoprotection in our skin, hair and eyes. It is also found in the *substantia negra* of primates, is a powerful antioxidant, metal chelator and free radical scavenger.[32] Apart from its biological relevance, melanin and related molecules (*e.g.* poly dopamine)[36–38] have emerged as functional materials in applications such as supercapacitors,[39] batteries[40] and even optoelectronics.[41] Bothma *et al.*[42] first showed that melanins could be processed into 'device quality thin films' with film thicknesses from 10 s of nanometres to microns. More recently, a range of processing techniques have been developed to do likewise using appropriate solvents and spin casting.[34,39,41] It is also now well established that melanin is a hybrid electronic-ionic conductor with the dominant charge carrier being the proton.[33–35] The origin of these transport properties is a local redox reaction called the comproportionation equilibrium (Fig. 1). In this reaction, two quinone moieties of different oxidative states react together with adsorbed water from the environment to form an intermediate oxidative state and in so doing releasing protons. The released protons 'hop' *via* the Grötthus mechanism site-to-site through the hydrogen bonded water network with maximum mobilities of order 10^{-3} cm^2 V^{-1} s^{-1}. This is analogous to the diffusion of an electronic hole in a disordered molecular semiconductor, and as such for several decades melanin was thought to be a p-type amorphous semiconductor.[32,33,43] The ability of melanin to be processed, deposited and patterned, plus its properties as a biocompatible proton source and conductor, lead us to hypothesize that it could be used as a solid-state ionic gate in a miniaturised electrochemical transistor.

Herein we show how these melanin gates can be incorporated into 100 μm channel length PEDOT:PSS-based transistors, forming an all-solid-state device. We demonstrate unequivocally that they can reliably modulate the channel conductance under low voltage operation with on/off ratios exceeding 10^4. The gating is volumetric and we observe very high channel capacitances greater than 200 F cm^{-3}.

Results

An all-solid-state melanin-OECT operating under ambient conditions

A critical step in the transistor fabrication was the deposition of a Hexamethyldisilozane (HMDS) monolayer on top of the channel prior to coating the gate. The HMDS hydrophobically

modified the PEDOT:PSS which otherwise would have re-dissolved in the basic pH, aqueous melanin deposition solution causing shorting between gate and source–drain contacts. The entire device structure is shown schematically in the inset of Fig. 2 and the melanin gate was contacted using a gold top electrode thermally evaporated at low energy such as not to cause electrode ingress.

In the first instance, these transistors were tested under ambient laboratory conditions in a standard manner by obtaining forward and back sweep transfer (Fig. 2a and Fig. S1, ESI†) and output (Fig. 2b and Fig. S2, ESI†) characteristics. These ambient laboratory conditions provided enough natural moisture to render the melanin 'conducting', i.e. sufficient water to facilitate proton percolation[33] and hence test the solid-state gating concept. The transfer curve (Fig. 2a) reveals that at zero gate voltage ($V_g = 0$ V) the transistor is in the 'On' state with high current flows through the channel (I_d). Upon application of a small positive gate voltage

(≈ 1 V), the transistor turns 'Off'. This behaviour is consistent with protons moving into the PEDOT:PSS, electrochemically de-doping and reducing the number density of free carriers available for conduction across the polymer backbone. The output characteristics in Fig. 2b confirm p-type channel behaviour: in general, the relationship between I_d and source–drain voltage (V_d) is almost linear for low V_d and all applied V_g, and with the application of larger negative V_d the current begins to saturate depending on V_g. In addition, Fig. 2b shows almost complete channel turn-off with modest gate voltages (<1.0 V).

These transfer characteristics were obtained at $V_d = 100$ mV at a delay time of 1 s (1 data point per second). The inset shows a schematic of the device and a simple demonstration of the proposed operational principle. In Fig. 2a (and indeed Fig. 2b), forward-back scan hysteresis is clearly visible. This is not unexpected in a device whose dynamics and operational principles originate from drift of ions (protons) under an applied field: the melanin gate is in essence a capacitor. To demonstrate this principle, we varied the delay time (the time between data points). One would naturally expect the hysteresis to increase significantly with shorter delay times. This is indeed the case as shown in Fig. S3 (ESI†), and at the shortest delay time (100 ms between data points), the device does not even turn off completely due to persistence of the space charge. The lowest degree of hysteresis and complete device turn off is obtained at a delay time of 5 s. These behaviours are consistent with the proposed mechanism of proton injection into the PEDOT:PSS gate. To add further credence to this assertion we then attempted to prove the melanin gate to be a proton source (as merely opposed to an inductive dielectric) by varying the proton concentration.

Melanin as a proton source – OECT behaviour as a function of hydration

As previously discussed, the electrical conductivity of melanin in various solid-state forms is strongly dependent upon its degree of hydration. This behaviour stems from the equilibrium shown in Fig. 1 and can be simply understood as an increase in the number of free carriers (protons) with increased water content. Further, and dependent upon local microstructure and density, the electrical conductivity appears to undergo a percolation transition at ≈ 9–12% by weight hydration as a continuous water network is formed to facilitate complete site-to-site hopping.[33,44] Thus, we would predict that as the melanin top gate of our OECT is hydrated, we should observe:
   (i) an increased on/off ratio;
   (ii) a lower turn on/off gate voltage;
   (iii) lower source–drain current at a specific gate voltage; and
   (iv) a higher channel transconductance (g_m).

To test these predictions we created a hydration chamber and deployed a point contact liquid metal gate electrode EGaIn: a gallium–indium alloy which is liquid at room temperature and commonly used in the electronics industry. This enabled exposure of the melanin top gate to a controlled hydrating atmosphere without the capping gold contact, and OECT characteristics to be obtained after the attainment of adsorption equilibrium.[44]
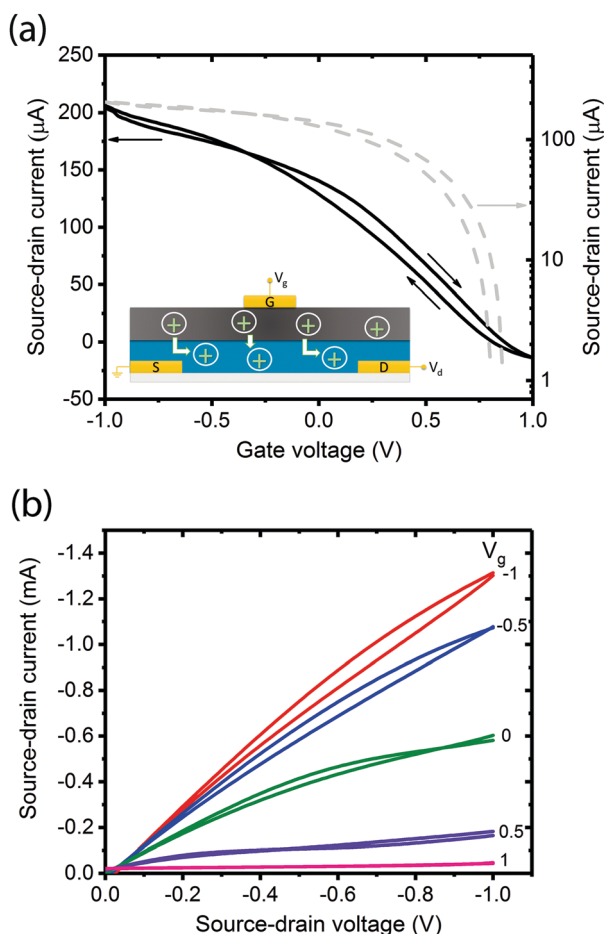

Fig. 2 (a) Transistor transfer characteristic of a PEDOT:PSS channel (100 nm thick film, 100 μm channel length), melanin top gate and gold gate electrode, solid state OECT. On/off ratio approximately 10^2. Inset shows schematic in which blue corresponds to the PEDOT:PSS channel, dark grey to the melanin gate and S, D and G are the source, drain and gate electrodes respectively. Proton injection from the melanin top gate de-dopes the PEDOT:PSS channel reducing the source–drain current. (b) Transistor output characteristic. The device behaves as a p-type transistor and as would be expected for positive ion injection.
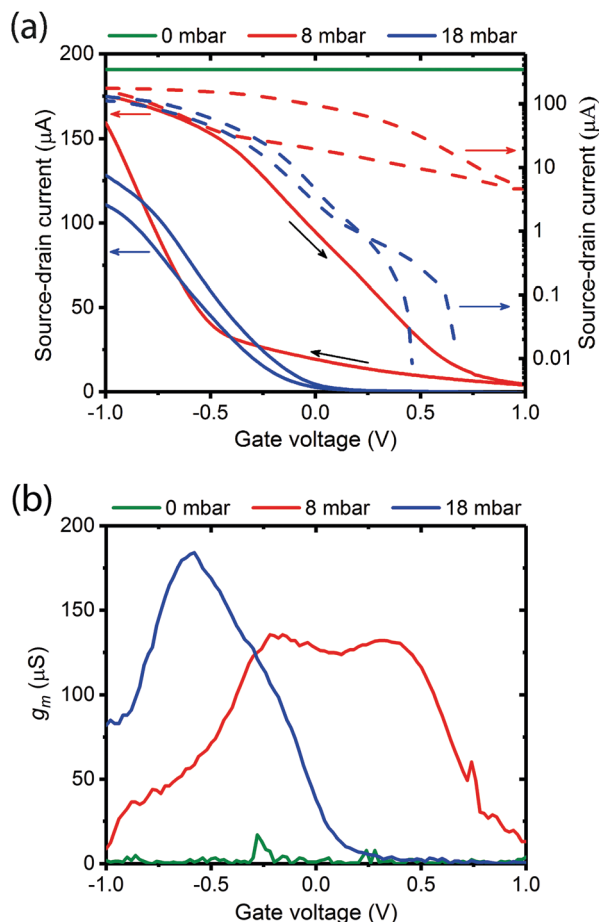
Fig. 3 (a) Hydration dependent transfer characteristics of a melanin-based OECT at 0 mbar water vapour pressure (green line), 8 mbar (red line) and 18 mbar (blue line). On/off ratio is approximately 220 at 8 mbar and approximately 10^4 at 18 mbar pressure. The noise at 0 mbar is negligible compared with the scale of the transfer curves. (b) The corresponding transconductance (forward sweep), which reaches 175 µS at its peak.

Fig. 3a shows typical transfer characteristics of a device measured at different vapour pressures of water (0 mbar – dry; 8 mbar – low hydration below the percolation transition; 18 mbar – high hydration and above the percolation transition). The corresponding output curves are provided in Fig. S4 (ESI†). We note the following:

(1) when the gate is dry there is no transistor behaviour;

(2) there is a dramatic decrease in source–drain current and transistor characteristics are recovered at low hydrations (8 mbar);

(3) the transistor turn off voltage decreases considerably at 18 mbar (0.2 V) versus 8 mbar (1.0 V); and

(4) the on/off ratio increases from ≈ 20 at 8 mbar to $> 10^4$ (comparable with a liquid gate OECT) at 18 mbar with V_d held again at 100 mV.

The ratio of the change in I_d versus change in V_g is known as the channel transconductance (g_m). It is essentially the first derivative of the transfer characteristics and is used as an indication of device sensitivity, and a measure of the transistor switching voltage range. Fig. 3b shows the transconductances

derived from Fig. 3a for the three hydration levels. As predicted the transconductance increases and the voltage operating range narrows as the gate hydration is increased. A maximum transconductance of ≈ -175 µS was recorded at −0.5 V and 18 mbar pressure. These observations agree with our predictions, and strongly support the assertion that the melanin is acting as a proton source and injecting gate.

Mechanism – direct injection channel modulation

In addition to the predictions and observations outlined above, we now test whether this device is a true OECT rather than some novel organic field effect transistor (OFET) where the channel is inductively gated.[14] Rivnay et al.[45] recently demonstrated that the key difference between an OECT and an OFET is the role of capacitance. In an OFET, the surface capacitance of the dielectric/channel interface is paramount, while for the OECT the volumetric capacitance of the channel is the main operational driver. In the latter case, the 'thickness' of the PEDOT:PSS layer forming the channel becomes a relevant control parameter, and the basic transistor equations defining the source–drain current (I_d) and transconductance can be written:

$$I_d = (W\mu/L)dC_p^*[V_T - V_G + V_d/2]V_d \tag{1}$$

$$g_m = (W\mu/L)dC_p^*[V_T - V_G] \tag{2}$$

where W, L and d are the width, length and thickness of the channel, μ is the hole mobility of the channel, C_p^* is the volumetric capacitance of the channel, V_T the threshold voltage, and g_m is the transconductance under saturation conditions.

To demonstrate that the volumetric capacitance is the active driving parameter in our devices (and hence confirm OECT operation), we performed an additional set of experiments whereby we measured the total charge injected for different channel thicknesses (Fig. 4a). There is a clear linear behaviour for each channel thickness confirming volumetric capacitance, noting that surface capacitive gating would have yielded a thickness independence. The volumetric capacitance can be determined from the slope of these charge-thickness plots, and for a liquid gated OECT this parameter remains constant.[45] However, we observe slightly different slopes and hence volumetric capacitances as a function of channel thickness, and assign this behaviour to the fact that the PEDOT:PSS and melanin top gate should be considered as two capacitors in series. This requires a modification of the model represented by eqn (1) and (2). A full derivation of this generalized two-capacitor OECT model is given in the ESI,† and the equivalent circuit shown as an inset in Fig. 4B. The modified transistor equations are thus:

$$I_d = (W\mu/L)d\alpha C_p^*\left[\frac{V_T}{\alpha} - V_G + V_d/2\right]V_d \tag{3}$$

$$g_m = (W\mu/L)d\alpha C_p^*\left[\frac{V_T}{\alpha} - V_G\right] \tag{4}$$

where $\alpha = C_m^*t/(C_m^*t - C_P^*d)$, C_m^* is the volumetric capacitance of the melanin top gate, and t its thickness. Given this
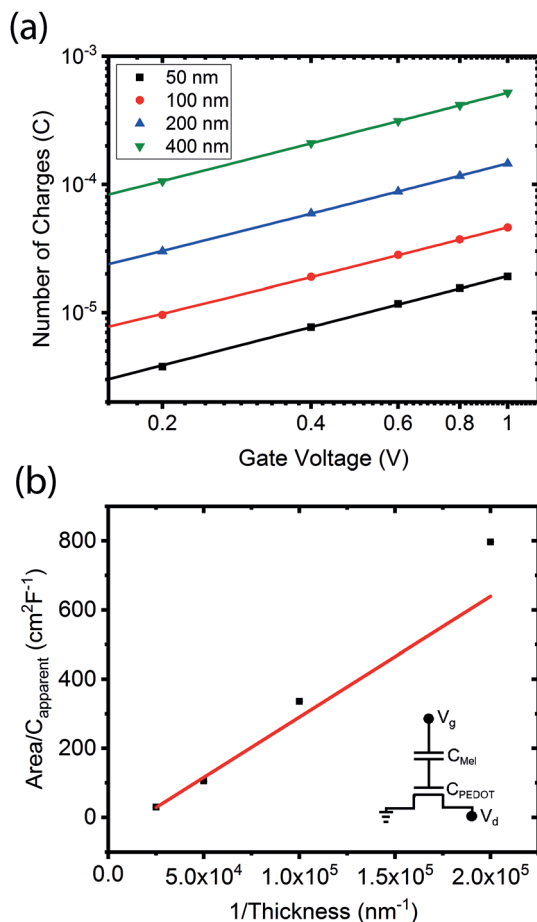
(a)

(b)

Fig. 4 Capacitance measurements. (a) Charge injected into the OECT channel as a function of V_g for different PEDOT:PSS channel thicknesses while maintaining a melanin top gate of 70 nm. (b) The inverse capacitance against inverse thickness of the PEDOT:PSS channel. Inset shows our device to be a transistor with a two capacitor gate.
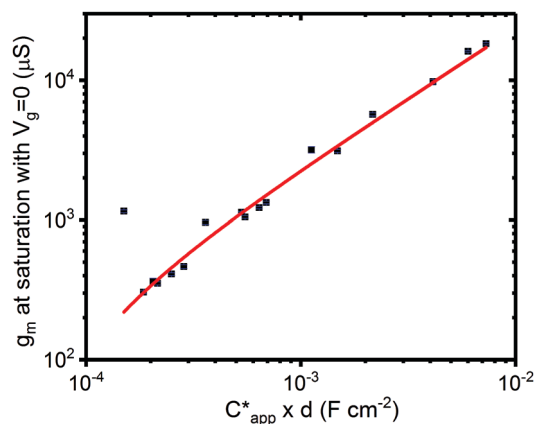

Fig. 5 Transconductance at saturation. Transconductance at saturation calculated from the measured output characteristics (at $V_g = 0$ V) for multiple devices with different channel thicknesses. The red line shows a linear fit as predicted from eqn (3) and (4).

modification, we can use Kirchoff's laws to determine the capacitances of the melanin and PEDOT:PSS gate and channel (also described in the ESI†) and the results of that analysis are shown in Fig. 4b (inverse apparent capacitance *versus* inverse channel thickness). From the slope of Fig. 4b we obtain a volumetric capacitance for the PEDOT:PSS channel of 224 ± 14 (2SE) F cm^{-3} and thus from α the melanin gate capacitance of -1420 ± 470 (2SE) F cm^{-3} ($t = 70$ nm).

Discussion

The results outlined above do confirm that we have achieved volumetric gating in the OECT-based melanin-PEDOT:PSS transducer. In general our capacitance measurements are also consistent with expectations. We do however note that our PEDOT:PSS volumetric capacitance is higher than reported by Rivnay *et al.*[45] by an order of magnitude. This difference can be simply understood by observing that the PEDOT:PSS in our devices was used as is, and not modified as in ref. 45. The melanin top gate large capacitance is consistent with its reported supercapacitor properties.[39] The polarity (negative sign) is

indicative of the stabilisation of the semiquinone species (anions) under the operating conditions of the gate and is not an indication of ferroelectric behaviour. In addition, eqn (4) predicts that the transconductance at saturation (g_m) should vary linearly with channel thickness ($g_m \propto d \times \alpha C_p^*$, where αC_p^* is the apparent capacitance C_{app}^*). This is plotted in Fig. 5 for numerous devices and the relationship is indeed linear. Finally, it is worth noting that these results confirm that the aforementioned ENODe reported by van der Burgt *et al.* could indeed be functioning by direct cation injection into the postsynaptic electrode as proposed.[30] This underlines the importance of volumetric capacitance for low voltage operation of bioelectronic transducing interfaces. Like many reported transducing interfaces, it is important to note that our devices at this stage are merely proof of concept and have not been optimized for actual biological models and measurements. For example, the gold top contact for the device should be ultimately replaced by a biological target, which will act as the gate. Furthermore, the device architecture has not been optimised for frequency response, which will most likely be required to improve the response time. This will be a necessary step in order to sense at high frequency neuronal cell activity as has been noted for other interfaces.[31]

Bearing in mind that the reported devices are proof of concept, it is instructive to discuss their future potential by benchmarking performance against current PEDOT:PSS-based liquid OECTs. One figure of merit that can be used for bench-marking is the transconductance,[46] since it is the main transistor parameter that governs signal amplification. State of the art PEDOT:PSS based OECTs have been reported[45–48] with max-imum/peak transconductances of ≈ 5–20 mS and saturation transconductances of around 20 mS. For our devices with fully hydrated top gates, we achieved a maximum/peak trans-conductance of around 0.175 mS (see Fig. 3b) and trans-conductances at saturation (Fig. 5), depending on conductive channel thickness, of around 0.4–20 mS. However, we note that our most stable devices possessed channel thicknesses of

$\approx$100 nm, which yielded $\approx$1 mS saturation transconductance. Thus, our devices are currently 1 order of magnitude lower in transconductance than state-of-the-art OECTs. However, OECT transconductances depend on device geometry/aspect ratio, as a simple inspection of eqn (1)–(4) will show. These geometric considerations are well understood.[45] Our transistors have aspect ratios (Wd/L) in the range $4 \times 10^{-4} - 4 \times 10^{-3}$ μm. In contrast, as an example, Rivnay et al.[45] demonstrated devices in the range $5 \times 10^{-2} - 5$ μm. If we consider Rivnay et al.'s work as normative for what can be achieved easily with device engineering, then re-engineering our devices may increase the transconductance by a factor of 10^2, thus potentially surpassing current state-of-the-art devices by an order of magnitude.

These transconductance considerations have natural implications for transistor gain and hence sensitivity. OECT devices take a voltage input at the gate (ion signal) and translate it to a current signal at the drain.[46,47] In order to extract a voltage signal, a load resistor can be connected to the drain of the transistor, from which the gain can be determined. At saturation, gain = $|dV_L/dV_g| = g_m R_L$, where g_m is the transconductance at saturation and R_L is a load resistor that is connected across the drain.[46,47] Unfortunately, we did not operate our transistors in this drain resistor mode, but we can discuss the potential gain by reference to the transconductance. Our data in Fig. 5 is for saturation at $V_g = 0$ V. This makes it comparable with recently published work on determining the gain in PEDOT:PSS-based OECTs.[47] These devices, with saturation transconductance values around 5 mS, yielded approximate gains of $\approx$20 V/V. Assuming all else is equal, it would imply our stable devices may have an amplification of 4 V/V if similar loads were utilised. We note again that appropriate device engineering may yield devices of higher gain exceeding state-of-the-art. We estimate from our knowledge of the device scaling that a gain in the proton to electronic signal of around 100 V/V could be possible.

This potential for future performance promises new opportunities for direct bioelectronic transducing interfaces. Coupled with the solid-state architecture, real, functional devices that enhance and process signals, and which can be miniaturised, it opens up the exciting route of bioelectronic computing at the biological interface in vivo.

Conclusions

In conclusion, we have demonstrated a functional, all-solid-state electrochemical transistor which is capable of efficiently transducing proton-to-electron currents. The device is p-type and gated by the conducting biomacromolecule melanin. We achieve respectable on/off ratios of $\sim 10^4$ with low voltage operation (<1.0 V). These transducers operate by 'volumetric gating' – direct injection of protons into the semiconductor channel which modulates the channel current. We also present a generic transistor model to test and explain its operation, which should in principle be broadly applicable to all OECT architectures by the inclusion of multiple volumetric capacitances. This simple all-solid-state architecture is amenable to

miniaturization and a definitive step on the pathway to integrated bioelectronic logic.

Experimental section

Materials

Melanin was synthesized following a standard literature procedure,[49] utilizing as the initial starting material D,L-dopa (Sigma-Aldrich). D,L-dopa was dissolved in deionized water, subsequently adjusted to pH 8 using NH$_3$ (28%). Air was then bubbled through the solution under stirring for 3 days. The solution was then brought to pH 2 using HCl (32%) to precipitate the formed melanin. The aggregated solution was then filtered and washed multiple times with deionized water and dried. The obtained powder was re-dissolved to create a solution for thin film casting according to previous published work[42] the composition of which was $\approx$0.7 g melanin in 5 ml H$_2$O and 10 ml NH$_3$ (28%) (being stirred for 1 hour at room temperature and then ultrasonicated for 1 hour).

Device fabrication

Glass slides (15 mm $\times$ 15 mm) were cleaned with Alcanox, rinsed in deionized water and ultra-sonicated in acetone (5 min). Afterwards they were rinsed with deionized water, ultra-sonicated in 2-propanol (5 min) and dried under a flow of nitrogen. The substrates were finally treated with UV-Ozone (20 min). 5 nm Cr and 50 nm Au source and drain interdigitated electrodes (with the channel length and width, 100 μm and 11.2 mm respectively) were patterned using thermal evaporation. PEDOT:PSS (Clevios PH 1000, Heraeus Holding GmbH) films were then deposited on the substrates by spin-coating for 5 s at 500 rpm followed by 60 s at 1500 rpm and annealed for 15 min at 140 °C. A monolayer of Hexamethyldisilozane (ProScitech) was then spin coated on top of the PEDOT:PSS at 800 rpm for 60 s followed by 15 min annealing at 110 °C to act as a hydrophobic layer between PEDOT:PSS and melanin. A thin film of melanin was spin coated at 1500 rpm for 60 s. Finally, a 30 nm Au top gate contact was thermally evaporated. Capacitance measurements were performed using different thicknesses of PEDOT:PSS channel of 50 nm, 100 nm, 200 nm and 400 nm. All thicknesses were measured using a DEKTAK profilometer. Each sample consisted of 3 transistors with multiple samples fabricated for each type of experiment. Humidity dependent experiments were performed without gold top gate contact (see below for more detail).

Electrical measurements

The electrical characteristics of devices were measured using a probe-station and an Agilent Semiconductor Device Analyzer (B1500A). Transfer curves were obtained with V_d of 100 mV and V_g sweeping from -1 V to 1 V. The hold time for all measurements remained constant at 60 s. The influence of the delay time on the transfer characteristics of the devices was inspected using delay times of 100 ms, 200 ms, 500 ms, 1 s, 2 s and 5 s. All output curves were measured slowly enough to allow steady state to be reached (delay time 5 s, hold time 60 s). The stability

of devices was tested by performing multiple scan cycles, an example of which can be seen in Fig. S6a (ESI†). An example of the gate leakage current can be seen in Fig. S7a (ESI†).

Capacitance measurement were performed by measuring current *versus* time (total time 50 ms) of the gate and drain contacts as a function of V_g. The total charge was calculated by integration, and an example is shown in Fig. S5 (ESI†) for a 50 nm thick channel.

Humidity dependent experiments were performed in a vacuum capable chamber[44] using a custom made temporary contact system utilizing EGaIn (eutectic gallium–indium, Sigma-Aldrich) as a top gate electrode. The chamber was pumped down to a vacuum of $\approx 10^{-2}$ Torr for 2 hours using a rotary pump. The desired water pressure was reached by isolating the pump and bleeding in water (Milli-Q, freeze-that-pumped 3 times) vapour measured with a BOC-Edwards GK series (0–50 mbar) gauge. Each pressure was held for an hour to insure an equilibrium was reached in line with previously published work.[50,51] A cross check was performed by monitoring the source drain current over time to ensure equilibrium was achieved (Fig. S8, ESI†). After equilibration transistor devices were placed into contact with the liquid gate, and then the transistor characteristics were measured. Before increasing the pressure the top liquid gate contact was lifted to insure an equilibrium in the melanin film was reached for the next pressure. The stability of devices was also tested by performing multiple transfer cycles (see Fig. S6b, ESI†). An example of the gate leakage current can be seen in Fig. S7b (ESI†).

Funding

Author contributions

The work was conceived and supervised by P. M. Device fabrication and testing was performed by M. S. and analysis and theory led by A. B. M. who also contributed to project supervision. All authors contributed to manuscript writing.

Conflicts of interest

There are no conflicts to declare.

Acknowledgements

Notes and references

1 M. Berggren and A. Richter-Dahlfors, *Adv. Mater.*, 2007, **19**, 3201.
2 P. Meredith, C. J. Bettinger, M. Irimia-Vladu, A. B. Mostert and P. E. Schwenn, *Rep. Prog. Phys.*, 2013, **76**, 034501.
3 J. Rivnay, R. M. Owens and G. G. Malliaras, *Chem. Mater.*, 2014, **26**, 679.
4 P. Lin and F. Yan, *Adv. Mater.*, 2012, **24**, 34.
5 A. Noy, *Adv. Mater.*, 2011, **23**, 807.
6 K. Svennersten, K. C. Larsson, M. Berggren and A. Richter-Dahlfors, *Biochim. Biophys. Acta, Gen. Subj.*, 2011, **1810**, 276.
7 M. Muskovich and C. J. Bettinger, *Adv. Healthcare Mater.*, 2012, **1**, 248.
8 R. M. Owens and G. G. Malliaras, *MRS Bull.*, 2010, **35**, 449.
9 G. Tarabella, F. M. Mohammadi, N. Copped, F. Barbero, S. Iannotta, C. Santato and F. Cicoira, *Chem. Sci.*, 2013, **4**, 1395.
10 K. Xu, *Chem. Rev.*, 2004, **104**, 4303.
11 M. A. Ratner and D. F. Shriver, *Chem. Rev.*, 1988, **88**, 109.
12 N. F. Mott and E. A. Davis, *Electronic processes in non-crystalline materials*, Clarendon Press, 1979.
13 T. Miyake and M. Rolandi, *J. Phys.: Condens. Matter*, 2016, **28**, 023001.
14 G. Horowitz, *Adv. Mater.*, 1998, **10**, 365.
15 C. A. Angell, C. Liu and E. Sanchez, *Nature*, 1993, **362**, 137.
16 Z. Gadjourova, Y. G. Andreev, D. P. Tunstall and P. G. Bruce, *Nature*, 2001, **412**, 520.
17 M. Rikukawa and K. Sanui, *Prog. Polym. Sci.*, 2000, **2000**, 1463.
18 M. A. Hickner, *Mater. Today*, 2010, **13**, 34.
19 K. Tybrandt, K. C. Larsson, A. Richter-Dahlfors and M. Berggren, *Proc. Natl. Acad. Sci. U. S. A.*, 2010, **107**, 9929.
20 Y. Cui, Q. Wei, H. Park and C. M. Lieber, *Science*, 2001, **293**, 1289.
21 N. Misra, J. A. Martinez, S. J. Huang, Y. Yinmin Wang, P. Stroeve, C. P. Grigoropoulos and A. Noy, *Proc. Natl. Acad. Sci. U. S. A.*, 2009, **106**, 13780.
22 C. Zhong, Y. Deng, A. F. Roudsari, A. Kapetanovic, M. P. Anantram and M. Rolandi, *Nat. Commun.*, 2011, **2**, 476.
23 H. S. White, G. P. Kittlesen and M. S. Wrighton, *J. Am. Chem. Soc.*, 1984, **106**, 5375.
24 D. A. Bernards, G. G. Malliaras, G. E. S. Toombes and S. M. Gruner, *Appl. Phys. Lett.*, 2006, **89**, 053505.
25 P. Lin, F. Yan and H. L. W. Chan, *ACS Appl. Mater. Interfaces*, 2010, **2**, 1637.
26 D. A. Bernards, D. J. Macaya, M. Nikolou, J. A. DeFranco, S. Takamatsu and G. G. Malliaras, *J. Mater. Chem.*, 2008, **18**, 116.
27 D. J. Kim, N. E. Lee, J. S. Park, I. J. Park, J. G. Kim and H. J. Cho, *Biosens. Bioelectron.*, 2010, **25**, 2477.
28 P. Lin, X. Luo, I. M. Hsing and F. Yan, *Adv. Mater.*, 2011, **23**, 4035.
29 P. Leleux, J. Rivnay, T. Lonjaret, J. M. Badier, C. Benar, T. Herve, P. Chauvel and G. G. Malliaras, *Adv. Healthcare Mater.*, 2015, **4**, 142.

30 Y. van de Burgt, E. Lubberman, E. J. Fuller, S. T. Keene, G. C. Faria, S. Agarwal, M. J. Marinella, A. A. Talin and A. Salleo, *Nat. Mater.*, 2017, **16**, 414.

31 D. J. Carrad, A. B. Mostert, A. R. Ullah, A. M. Burke, H. J. Joyce, H. H. Tan, C. Jagadish, P. Krogstrup, J. Nygard, P. Meredith and A. P. Micolich, *Nano Lett.*, 2017, **17**, 827.

32 P. Meredith and T. Sarna, *Pigm. Cell Res.*, 2006, **19**, 572.

33 A. B. Mostert, B. J. Powell, F. L. Pratt, G. R. Hanson, T. Sarna, I. R. Gentle and P. Meredith, *Proc. Natl. Acad. Sci. U. S. A.*, 2012, **109**, 8943.

34 J. Wünsche, Y. Deng, P. Kumar, E. Di Mauro, E. Josberger, J. Sayago, A. Pezzella, F. Soavi, F. Cicoira, M. Rolandi and C. Santato, *Chem. Mater.*, 2015, **27**, 436.

35 M. R. Powell and B. Rosenberg, *Bioenergetics*, 1970, **1**, 493.

36 H. Lee, S. M. Dellatore, W. M. Miller and P. B. Messersmith, *Science*, 2007, **318**, 426.

37 H. Lee, B. P. Lee and P. B. Messersmith, *Nature*, 2007, **448**, 338.

38 Y. Liu, K. Ai and L. Lu, *Chem. Rev.*, 2014, **114**, 5057.

39 P. Kumar, E. Di Mauro, S. Zhang, A. Pezzella, F. Soavi, C. Santato and F. Cicoira, *J. Mater. Chem. C*, 2016, **4**, 9516.

40 Y. J. Kim, W. Wu, S. Chun, J. F. Whitacre and C. J. Bettinger, *Proc. Natl. Acad. Sci. U. S. A.*, 2013, **110**, 20912.

41 M. Ambrico, N. F. D. Vecchia, P. F. Ambrico, A. Cardone, S. R. Cicco, T. Ligonzo, R. Avolio, A. Napolitano and M. d'Ischia, *Adv. Funct. Mater.*, 2014, **24**, 7161.

42 J. Bothma, J. de Boor, U. Divakar, P. Schwenn and P. Meredith, *Adv. Mater.*, 2008, **20**, 3539.

43 J. McGinness, P. Corry and P. Proctor, *Science*, 1974, **183**, 853.

44 A. B. Mostert, B. J. Powell, I. R. Gentle and P. Meredith, *Appl. Phys. Lett.*, 2012, **100**, 093701.

45 J. Rivnay, P. Leleux, M. Ferro, M. Sessolo, A. Williamson, D. A. Koutsouras, D. Khodagholy, M. Ramuz, X. Strakosas, R. M. Owens, C. Benar, J. M. Badier, C. Bernard and G. G. Malliaras, *Sci. Adv.*, 2015, **1**, e1400251.

46 D. Khodagholy, J. Rivnay, M. Sessolo, M. Gurfinkel, P. Leleux, L. H. Jimison, E. Stavrinidou, T. Herve, S. Sanaur, R. M. Owens and G. G. Malliaras, *Nat. Commun.*, 2013, **4**, 2133.

47 M. Braendlein, T. Lonjaret, P. Leleux, J. M. Badier and G. G. Malliaras, *Adv. Sci.*, 2017, **4**, 1600247.

48 J. Rivnay, P. Leleux, M. Sessolo, D. Khodagholy, T. Herve, M. Fiocchi and G. G. Malliaras, *Adv. Mater.*, 2013, **25**, 7010–7014.

49 C. C. Felix, J. S. Hyde, T. Sarna and R. C. Sealy, *J. Am. Chem. Soc.*, 1978, **100**, 3922.

50 A. B. Mostert, K. J. P. Davy, J. L. Ruggles, B. J. Powell, I. R. Gentle and P. Meredith, *Langmuir*, 2010, **26**, 412.

51 A. J. Clulow, A. B. Mostert, M. Sheliakina, A. Nelson, N. Booth, P. L. Burn, I. R. Gentle and P. Meredith, *Soft Matter*, 2017, **13**, 3954–3965.